

OCTAVE, a bioinspired visuo-motor control system for the guidance of Micro-Air-Vehicles

Franck RUFFIER and Nicolas FRANCESCHINI

Biorobotics, Movement and Perception Lab., CNRS/Univ. de la Méditerranée,
31, chemin Joseph Aiguier, 13402 Marseille Cedex 20, FRANCE

ABSTRACT

We have developed a visually based autopilot for Micro Air Vehicles (MAV), which we have called OCTAVE (Optical altitude Control sysTEm for Autonomous VEHICLES). First we built a miniature MAV and an indoor test-bed. The mini-helicopter is tethered to a whirling arm and rotates around a central pole equipped with ground-truth positioning sensors for experimental evaluation. The 100-gram rotorcraft lifts itself by means of a single rotor that can also be tilted forward (pitch) to give the craft a horizontal thrust component (propulsive force). The helicopter's eye is automatically oriented downwards over an environment composed of contrasting features randomly arranged on the floor.

Here we show the feasibility of a ground avoiding system based on a low complexity opto-electronic system. The latter relies on an Elementary Motion Detector (EMD) that estimates the optic flow in the downward direction. The EMD functional structure is directly inspired by that of the fly's EMDs, the functional scheme of which has been elucidated at our Laboratory by performing electrophysiological recordings while applying optical microstimuli to the retina. The OCTAVE autopilot makes the aircraft capable of effective terrain following at various speeds: the MAV performs reproducible manoeuvres such as smooth cruise flight over a planar ground and hill climbing. The overall processing electronics is very light-weight, which makes it highly suitable for mounting on-board micro air vehicles with an avionic payload in the order of only a few grams.

Key words : Biorobotics, bioinspired vision, UAV (Unmanned Aerial Vehicle), MAV (Micro-Air-Vehicles), optic flow, visual guidance, AFCS (Automatic Flight Control System)

1. INTRODUCTION

The biorobotic approach initiated at our laboratory in 1985 [1-10] has led to designing, simulating and constructing biologically inspired sensors and control systems for the visual guidance of Micro-Air-Vehicles (MAV) [3, 5-9]. Attempting to transfer biological principles to robots is a useful way of finding viable solutions to arduous engineering problems while providing biology with fruitful returns [4, 10-11].

Conferring some autonomy and authority upon small aircraft (or micro-aircraft) is a challenging task that involves many issues such as the mass, energy and processing resources required. The authors of recent studies have addressed this problem by turning to biology [5-9, 12-16]. Some authors have performed insect-inspired visual guidance using panoramic vision on a blimp platform [15]. Ichikawa et al. have addressed the hover problem arising in the case of a 100-g model helicopter using basic motion detection [16]. Other projects have been based on more conventional computer-vision schemes [e.g., 17-20]. Amidi et al. have equipped their R50 Yamaha helicopter for performing all its manoeuvres (even the riskiest ones such as hovering and landing) on the basis of visual landmarks and accurate sensor fusion, but the equipment required on-board led to a rotorcraft weighing no less than 67,000 grams [19-20].

Dealing with UAVs that weigh only between 1 and 100 grams requires finding alternative guidance schemes. We have come to see winged insects as valuable model systems for the dynamic stabilization and the visual guidance of artificial micro-flyers. Insects' Elementary Motion Detector (EMD) neurons are known to process the *optic flow* to perform autonomous visual guidance [21-23]. In 1986, Franceschini et al. designed some small opto-electronic angular velocity sensors (or EMDs) [24-25], the principle of which was based on the findings they had made on fly EMDs by performing electrophysiological recordings on single neurons while concomitantly applying optical microstimuli to single photoreceptor cells [26]. Meanwhile, these artificial neurons have been used to equip several small robots at the {ruffier, franceschini}@laps.univ-mrs.fr; phone +33 491 16 41 29; fax +33 491 22 08 75; www.laps.univ-mrs.fr

Laboratory [e.g., 1, 2, 5, 7, 9]. In 1994, the Laboratory's first optic flow based altitude control simulation studies were published [3]. Netter and Franceschini's tethered 850-gram helicopter was able to perform basic obstacle avoidance on the basis of a retina feeding signals to 19 EMDs [6-7]. Biologically inspired microrobotics has also led to the development of a new visual sensor, called OSCAR, which enables a 100-gram tethered MAV to robustly perform tasks such as visual fixation and tracking in the presence of disturbances [5]. Recently, we redesigned the EMD circuit to obtain a lighter version (0.8-grams) [8].

The missions of future micro-air vehicles will require them to be agile enough to navigate safely in tight environments such as urban canyons, forests, industrial plants, construction works, or inside buildings. The Automatic Flight Control System (AFCS) described here, which we call OCTAVE (Optical altitude Control sysTEM for Autonomous VEHICLES) enables a minimalistic electronic system inspired by insects to guide an aerial vehicle automatically on the basis of its sight, without any need for a remote pilot to take care of the obstacles. The pilot (or a system having some authority) just needs to set two parameters: the speed (via the pitch angle) and an optic flow reference value. Both parameters will determine the height at which the robot will fly above the ground.

In section 2, we describe the visuo-motor control loop. Section 3 focusses on the bioinspired visual processing system. In section 4, we describe the micro-air-vehicle and the whirling arm to which it is tethered. Lastly, we present the experimental results obtained in a terrain following task.

2. VISUAL GUIDANCE STRATEGY

2.1. Optic flow under pure translation over a terrain

An eye-bearing MAV flying in pure translation over an unknown terrain (Figure 1) generates a translational optic flow Ω :

$$\Omega = \frac{v_x}{D} \sin\varphi \quad (1)$$

where v_x is the speed (ground speed) of the aircraft with respect to the ground, D its distance from the ground point and φ the angle between the gaze direction and the horizontal heading direction.

The optic flow generated is very small around the direction of self-motion ($\varphi = 0^\circ$), which is a pole of the optic flow field [27, 21], and grows larger in the periphery. The largest optic flow is encountered at an angle of 90° from the pole. We orient the robot's eye downwards ($\varphi=90^\circ$) so that D becomes the local altitude h (Figure 1b). Under these

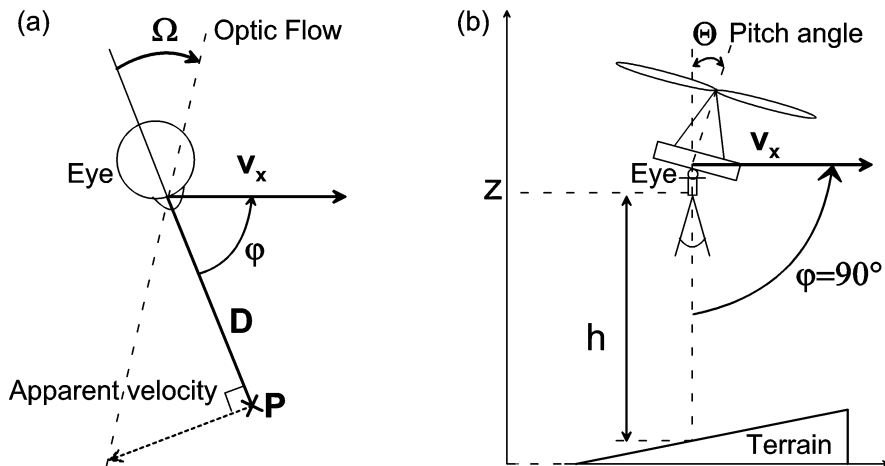


Figure 1. (a) Translation of an eye (at velocity v_x) over a contrast point P located at distance D and elevation φ generates an angular retinal velocity Ω , called the optic flow. (b) A micro-helicopter pitched forward by angle Θ flies at ground speed v_x . As the gaze direction is maintained vertically downwards, D becomes h , the distance above the terrain.

conditions, the optic flow range is maximized but Ω still depends jointly on the altitude and the ground speed.

$$\Omega = \frac{v_x}{h} \quad \text{when} \quad \varphi=90^\circ \quad (2)$$

2.2. Bio-inspired OCTAVE principle

The guidance strategy proposed here is inspired by the hypothesis made 50 years ago [28] that locusts control their altitude on the basis of the retinal slip speed in the ventral part of their compound eye. Locusts' behavior was taken to consist in maintaining a steady retinal angular velocity. More recently, by analyzing the flight behavior of the free-flying fruitfly (*Drosophila*), David noticed a relationship between flight speed and body angle [29]. The direction of the lift force generated by the two wings is mainly governed by the body pitch angle. The horizontal component of the lift (i.e., the propulsive force, which causes the forward motion and determines the flight speed) therefore depends on the body pitch angle as well. Pitch angle and lift are also the key parameters in the OCTAVE system that guides our miniature rotorcraft. The vectored propulsion mode we use, which consists in controlling only the direction (pitch angle) and the amplitude of the lift vector on the rotorcraft (see Section 4), can be compared with the propulsion mode used by the fruitfly.

2.3. OCTAVE visuo-motor control loop

The OCTAVE Automatic Flight Control System (AFCS) was designed by servoing the optic flow (Figure 2). This strategy is different from the other strategies classically used in aerospace research, such as altitude servoing (by means of a radio altimeter sensor, for instance) or ground speed servoing (by means of a laser velocimeter sensor, for instance).

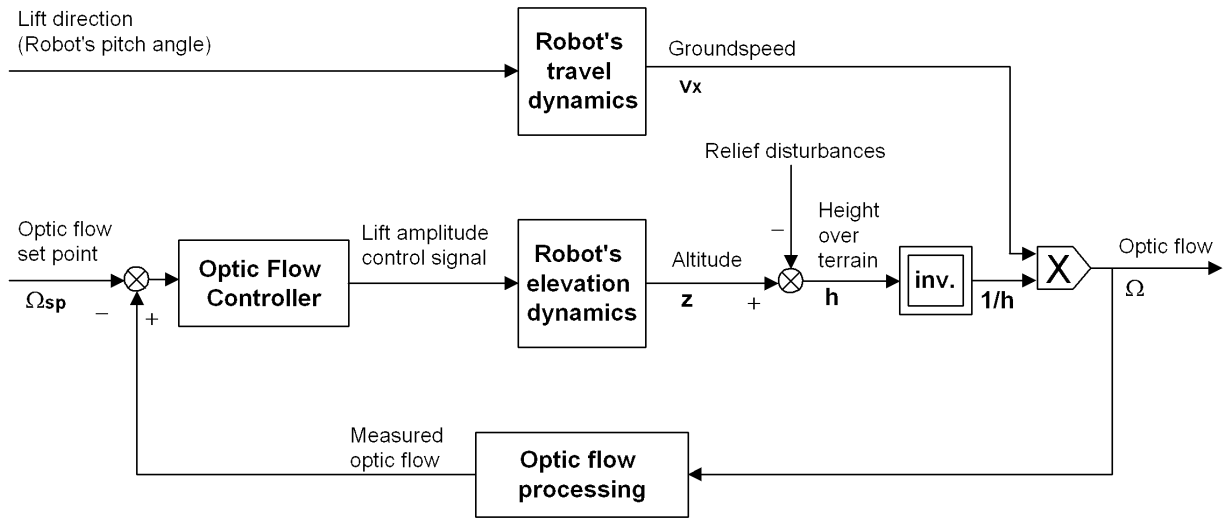


Figure 2. The OCTAVE system controls two inputs on the robot's dynamics: the direction of the lift vector, which determines the groundspeed v_x , and the amplitude of the lift vector, which determines the altitude z . In the results presented in this paper, the lift direction is set at a constant value and the lift amplitude results from the optic flow servoing.

The robot reacts to variations in the optic flow by controlling its lift via the rotor speed (roll per minute, *rpm*). At a given robot's pitch, any increase in the optic flow is interpreted as a decrease in the height h above the ground (see the signs of the signals at the comparator, fig. 2, left). This causes the rotor *rpm* to increase until an height h over ground is reached which re-establishes the required optic flow. Any change in relief is a disturbance for the feedback loop. The visual loop will thus ensure that a "safe height" is maintained by increasing the lift so as to raise the aerial robot above the obstacle until the optic flow reference value has decreased sufficiently.

At a given optic flow set point, the safe height h will rise appropriately with the ground speed v_x . This visual control loop scheme is a simplified version of the complex visuo-motor + aero-mechanical system. In our analysis of the visuo-motor control loop, we focussed on the travel and elevation dynamics.

There are two main external inputs to the OCTAVE system :

- **The lift direction (robot's pitch angle)**

The pitch angle determines the aerial robot ground speed. By keeping it constant, the ground speed v_x is kept fairly constant and enables the visuo-motor control loop to interpret any variations in the optic flow as variations in height h over the terrain.

- **The optic flow set point**

This input defines the ratio between the ground speed v_x and the height h above the ground. We can regard it as a safety (or confidence) parameter: the lower the optic flow set point, the higher the cruise altitude will be.

3. BIO-INSPIRED OPTIC FLOW PROCESSING

The optic flow processing is carried out by two devices (Figure 3):

- An elementary eye which transforms the optic flow Ω generated by the robot's forward motion into a temporal delay Δt between the responses of two neighboring photoreceptors, which is an inverse function of Ω .
- An Elementary Motion Detector (EMD) which processes this temporal delay Δt in a nonlinear way to estimate the optic flow Ω .

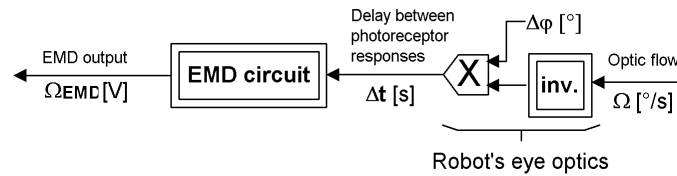


Figure 3. The optic of the eye transforms the optic flow Ω into a delay Δt between the photoreceptor responses. The EMD assesses the optic flow by processing this delay Δt in a nonlinear way [24-25].

3.1. Eye geometry

The elementary retina consists of just two photoreceptors Ph1 and Ph2 (Figure 4a). Their visual axes are separated by an interreceptor angle called $\Delta\phi$, the value of which (about 4°) is similar to that which exists between two visual units in the fruitfly eye [30]. The angular sensitivity of a lens + photosensor device is defined by a bell-shaped function characterized by its acceptance angle $\Delta\rho$ (angular width at half height). Here, $\Delta\rho = 4^\circ$. This function performs the first basic step in visual processing: low-pass spatial filtering, with a beneficial anti-aliasing effect [30]. A bell-shaped angular sensitivity curve was obtained here by defocusing the lens [6].

When the image of a contrasting edge passes across the field of view of this minimalistic eye, the photoreceptor outputs V_{Ph1} and V_{Ph2} vary smoothly one after the other (Figure 4b), and the delay Δt between them is equal to the time taken

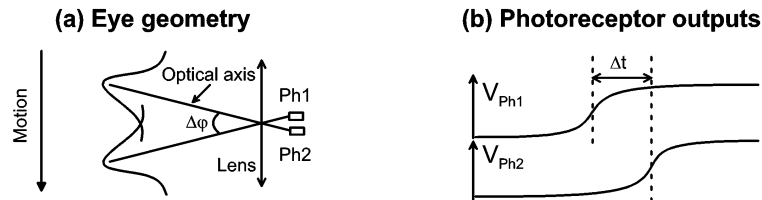


Figure 4. (a) A 8mm-diameter lens and 2 PIN photodiodes (Ph1 and Ph2) compose the elementary eye. Defocusing the lens creates a blur, which gives a Gaussian-like angular sensitivity for the photoreceptor, and this results in a beneficial low-pass spatial filtering [30]. The angle between the two optical axes is called $\Delta\phi$. (b) Moving a contrasting edge in front of the eye causes the two photoreceptors to respond similarly, but the one is delayed by Δt with respect to the other. The EMD processes these 2 photoreceptor outputs to give an estimate of the optic flow $\Omega = \Delta\phi \times \frac{1}{\Delta t}$.

by the contrasting edge to pass across both optical axes successively. Δt is inversely proportional to the relative angular speed Ω (or optic flow) :

$$\Delta t = \Delta \varphi \times \frac{1}{\Omega} \quad (3)$$

3.2. Insect-derived EMD processing and its implementation

The electronic EMD output, Ω_{EMD} , approximates the optic flow Ω .

$$\Omega_{EMD} \cong k\Omega = K' \frac{1}{\Delta t} \quad (4)$$

The original EMD scheme developed at our laboratory [24-25, 5] is a “token-matching scheme” [31]. It consists of several linear and nonlinear processing steps implemented by devices such as filters, rectifiers, threshold units and minimum detectors. The EMD processing consists in processing the time Δt at which the image of a given feature (“token”) passes across the lines of sight of two neighboring photoreceptors. The EMD output Ω_{EMD} decreases monotonically with Δt and therefore increases monotonically with Ω . Ω_{EMD} is maintained by a sample and hold circuit until the next EMD measurement. The responses of this velocity sensor are largely invariant with contrast, unlike the responses of correlation based EMDs [32].

Our current hybrid implementation of an EMD, which comprises both analog preprocessing and digital microcontroller-based processing, is a small module weighing only 0.8-grams [8], which could easily be mounted onboard the aerial robot. However, the robot’s behavior described here (Section 5) was obtained with an EMD circuit based on a *Field Programmable Analog Array* (FPAA by Anadigm), which was placed off-board [8].

4. EXPERIMENTAL SET-UP

4.1. Aerial robot

We built a small (100-gram) rotorcraft consisting of a rotor, a miniature electronic eye and its control electronics

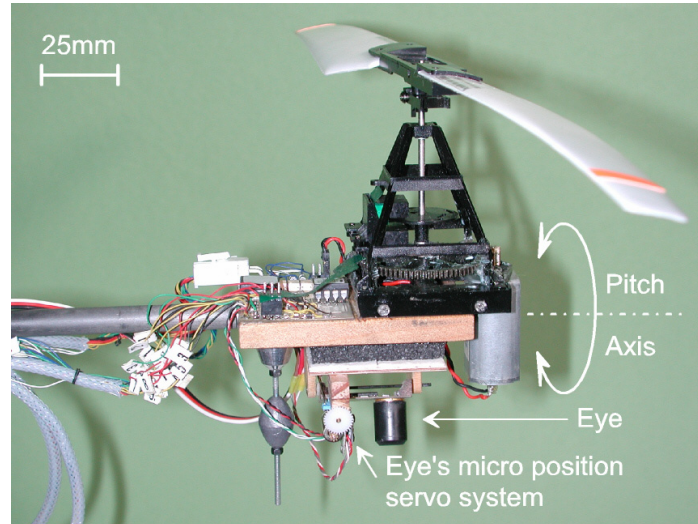


Figure 5. 100-gram miniature rotorcraft developed for testing the optic flow autopilot. A PWM-controlled DC motor drives the 30-cm-diameter, 5-gram propeller via a reducer. The robot is mounted at the end of the whirling arm shown in Figure 6 and can be oriented around its pitch axis by means of an external signal. This pitch axis remains horizontal at all altitudes, due to the pantographic design of the whirling arm. Static balance is achieved with a small lead placed under the main platform, which damps the mechanical vibrations. The electronic eye is mounted on an orientable 400 μ m-thick PCB, the pitch of which is controlled by a 2.4g position servo system. When the robot pitch angle changes, the micro-servo counterrotates the eye so as to keep the gaze oriented vertically downwards, as shown in figure 1b.

(Figure 5). This micro-air vehicle is based on the rotor mast of the Keyence “Revolutor” RC model helicopter. A DC motor controlled by Pulse Width Modulation (PWM) drives the fixed pitch propeller. An external control signal sets the rotorcraft pitch angle via a position servo system. A local control loop (not shown here) servo the rotor *rpm* to the input signal. The rotor *rpm* is sensed by an on-board opto-electronic sensor. An onboard 2.4 gram position servo system (Figure 5) orients the eye so as to maintain the gaze downward ($\phi=90^\circ$, in figure 1b) by automatically counter-rotating the eye to compensate for the pitch of the rotorcraft. For experimental convenience, we added a landing gear which extends $l=0.3\text{m}$ below the robot’s eye. The altitude plotted in the Results (section 5) therefore corresponds to $z-l$, the altitude of the landing gear.

4.2. Test-rig

The rotorcraft is tethered to the end of a light, counterbalanced whirling arm (Figure 6), which is driven in elevation and azimuth by the aircraft lift and propulsive forces, respectively. This arm actually consists of three parallel carbon/aramide fiber tubes forming a pantograph, as shown in [6], the function of which is to prevent any yaw and roll motion of the aircraft, which therefore has only three degrees of freedom: travel, elevation and pitch. The electrical signals to and from the aerial robot are channeled through a miniature 45-contact low friction slip-ring assembly mounted on the central pole of the whirling arm. This makes for unhindered, unlimited travel. Any increase in the rotor *rpm* causes the aerial robot to lift itself and rise. Any forward tilting of the rotor causes the robot to move forward. The mean circumference travelled by the MAV during one lap is about 12 meters. For the sake of convenience, we decided to plot the trajectories (Section 5) on a two dimensional plane defined by the horizontal distance traveled and the altitude.

A computer printed disc was laid over the ground to simulate a richly contrasting environment made of randomly ordered contrasting sectors (printed on a disc with a 4.5-meter outside diameter). The various sector widths correspond to a large spatial frequency range (from 0.06 to $1.75 \text{ c}/^\circ$ for $h=1\text{m}$), which is suitable for testing the robustness of the visual processing system. The actual edge contrast m was determined experimentally by measuring the relative luminance (I_1, I_2) of any pair of neighboring sectors and calculating:

$$m = \frac{I_1 - I_2}{I_1 + I_2} \quad (5)$$

As measured in the same (near IR) spectral range as that of interest in the robot’s eye (sensitivity peak $\lambda_{\text{max}}=850\text{nm}$), the effective edge contrast turned out to be relatively low (from 4% to 30%) on the printed disc. Part of the visual

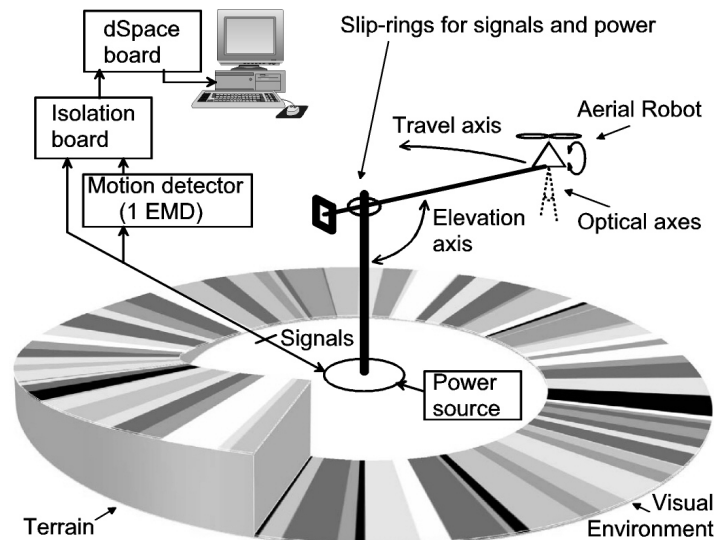


Figure 6. Test-rig composed of a pantographic whirling arm supporting the 100gram rotorcraft (Figure 5) which flies over a 4.5-meter outside diameter arena. The textured terrain below consists of randomly distributed, variously contrasting sectors. One third of this circular terrain consists of a ramp, which stops abruptly at the height of 50cm. This test-rig with a tethered MAV permits the essence of the OCTAVE autopilot to be demonstrated and tested reliably and reproducibly under safe conditions.

environment was mounted on a slanted surface (“circular ramp”). This relief creates a serious output disturbance in the OCTAVE loop and therefore provided a good means of testing its efficiency.

A PC equipped with an input/output DSP board (dSpace) coupled with MATLAB/Simulink was used to run the experiments in real time (without depending on the PC operating system), and to monitor the robot’s behavior via a servo-potentiometer on the elevation axis and an optical encoder on the travel axis. The experimenter commands the servo-motor that pitches the aerial robot forwards to attain the required speed.

4.3. OCTAVE control loop implementation

$G_{v_x}(s)$ gives the travel dynamics transfer function between the pitch angle Θ [°] and the ground speed v_x [m/s]. Since the pitch angle is maintained constant in this study, the robot’s trajectories are not subject to the travel dynamics.

$G_z(s)$, the elevation dynamics transfer function of the rotorcraft, was identified on the test-rig from the response to a step input. $G_z(s)$ gives the linear transfer between the DC motor control signal, u [V], and the altitude, z [m], around the operating point.

$$G_z(s) = \frac{Z(s)}{U(s)} = \frac{K_z \omega_z^2}{s^2 + 2\xi_z \omega_z s + \omega_z^2} \quad (6)$$

with $K_z=1.114$ m/V, $\xi_z=0.2239$ and $\omega_z=0.9511$ rad/s

A proportional derivative (PD) controller, $C_\Omega(s)$ was introduced into the feedback loop to raise the phase margin and increase the damping, and thus enhance the stability and shorten the response time. The PD controller also includes a low-pass filter which reduces the effects of short time errors on the EMD output and the high frequency components due to the hold between two EMD updates. This low-pass filter suitably decreases the jitter on the rotor control signal. The overall optic flow controller $C_\Omega(s)$, which runs on-line on the dSpace board, is :

$$C_\Omega(s) = K_C \left(\frac{\tau_1 s + 1}{\tau_2 s + 1} \right) \left(\frac{1}{\tau_3 s + 1} \right) \quad (7)$$

with $K_C=0.2592$ V.s/°, $\tau_1=1.5$ s, $\tau_2=0.12$ s, $\tau_3=0.25$ s

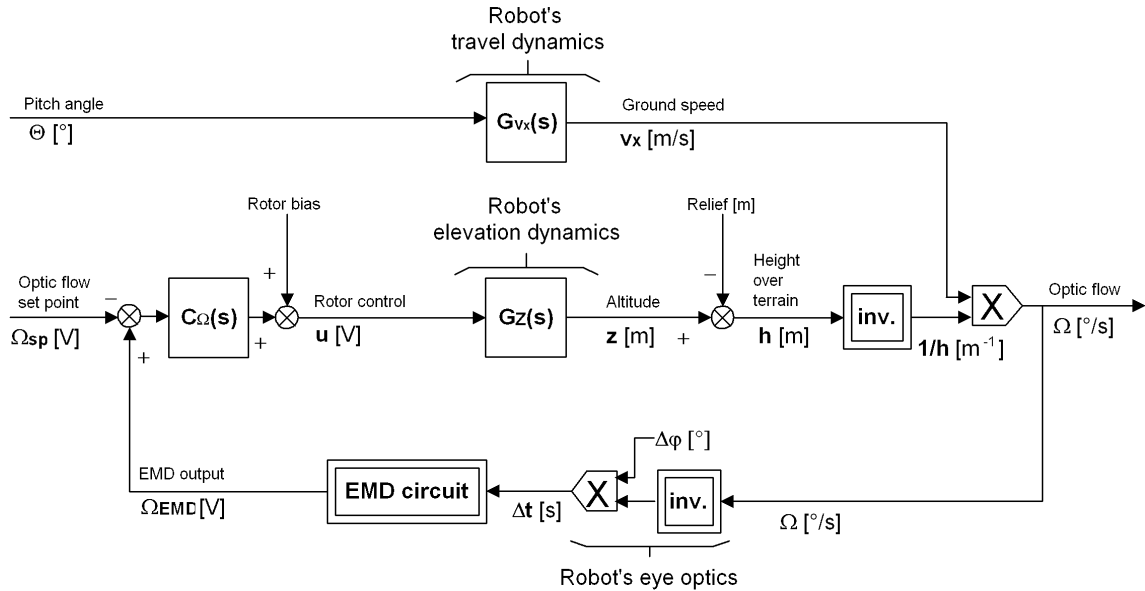


Figure 7. The optic flow controller $C_\Omega(s)$ which we incorporated into the loop regulates the optic flow Ω measured by an EMD circuit. When the EMD output Ω_{EMD} is higher than the optic flow set point Ω_{sp} , $C_\Omega(s)$ commands a higher rotor *rpm*. This leads to an increase in altitude, which induces a decrease in optic flow. The ground speed v_x is directly driven by the helicopter pitch angle. The ground speed v_x can be said to weigh the optic flow according to equ. (2).

We checked that the controller is robust to parametric variations in the 1 to 3m/s ground speed range and in the 0 to 2m altitude range. In the elevation dynamics $G_z(s)$, the gain K_z varies by $\pm 50\%$ with the rotor rpm and inversely with the flying speed. The pulsation ω_z and the damping factor ξ_z vary to a lesser extent. We suitably neglect the coupling between the rotor control signal, u [V], and the ground speed, v_x [m/s]. Our experimental results showed that this coupling is in fact very small (as can be inferred from the forward speed constancy observed in Figure 8b).

A local rotor speed control loop (not shown in Fig. 7) was used to improve the dynamic properties of the overall visuo-motor control system. It eliminates any local aerodynamic disturbances impinging on the rotor.

At low rotor control signal values, the MAV remains at altitude zero because it first needs enough lift to compensate for its own weight. This “dead zone” is compensated for by adding a bias signal to the rotor control signal (see Figure 7).

5. TERRAIN FOLLOWING RESULTS

5.1. Robot’s trajectories as a function of pitch angle

The robot’s altitude (Figure 8a) was monitored during one cycle of travel over the scene depicted in figure 6 and the trajectories recorded show that the robot followed the terrain smoothly at various ground speeds. The OCTAVE system thus causes the altitude of the robot to vary automatically as required by the changing relief of the land. Interestingly, the use of an optic flow scheme in the control loop automatically generates a “safe altitude” which conveniently increases with the ground speed: the faster the robot is moving, the further away from the obstacles it will be. The aerial robot equipped with OCTAVE adapts its altitude whatever the ground speed and the local height over the terrain, *although no explicit knowledge about the ground speed or the local altitude is available onboard the vehicle.*

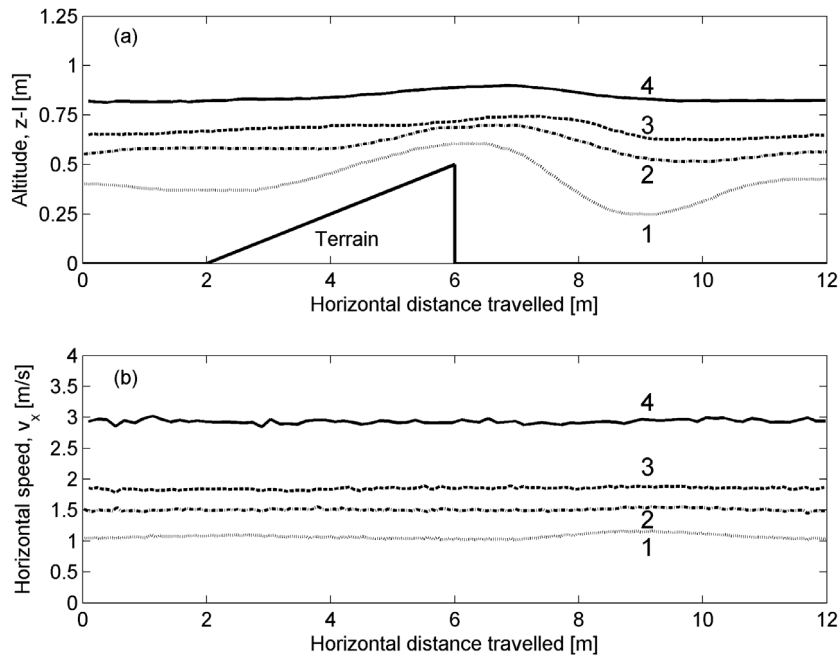


Figure 8. (a) Ground avoidance trajectories of the miniature rotorcraft recorded at four different ground speeds (1:1m/s; 2:1.5m/s; 3:1.8m/s; 4:3m/s). Here, the horizontal distance travelled plotted is that on the mean circular track and the altitude ($z-l$) is that of the landing gear, which is at distance $l = 0.3m$ under the eye (section 4.1). (b) The horizontal speed can be seen to have remained fairly constant throughout each trajectory. This shows that the coupling between rotor speed and ground speed can actually be neglected, as hypothesized in section 1.

5.2. Robot's trajectories as a function of the optic flow set point

The optic flow set point is the second input to the OCTAVE visuo-motor control system. As shown in Figure 9, OCTAVE makes the robot avoid the obstacle whatever the optic flow setting (the other parameters remain unchanged). The trajectories shown here were obtained at one and the same ground speed v_x (1m/s), but with four different optic flow set points. It can be seen here that each optic flow set point results in a flight at a different altitude. Flight at the highest altitude corresponds to the lowest optic flow set point (curve 4). On the contrary, the MAV hugs the ground all the more closely as its optic flow is set at a high value (curve 1).

Along all these trajectories, we can see that the control loop does not completely eliminate the disturbance brought about by the relief. This is also reflected in the fact that the EMD output does not remain constant throughout the lap (Figure 9b). Yet the responses of the closed loop system lead to efficient obstacle avoidance in any case.

The on-line optic flow update performed by the EMD is efficient despite the estimation errors which are mainly caused by mechanical vibrations and correspondence errors [33]. The closed loop OCTAVE system filters these errors so that they do not disturb the control loop: no jerky reactions can be observed on any of the four trajectories. On the other hand, the avoidance which occurs when the robot is rising above the obstacle is less pronounced at low optic flow reference values (curve 4) than at high reference values (curve 1). This is because changes in the relief affect the optic flow less when the height h is greater (due to the hyperbolic law between Ω and h , cf. Equation 2). Via its optic flow set point, the OCTAVE system enables the aerial robot to safely adapt to the difficulty or the unpredictability of the terrain.

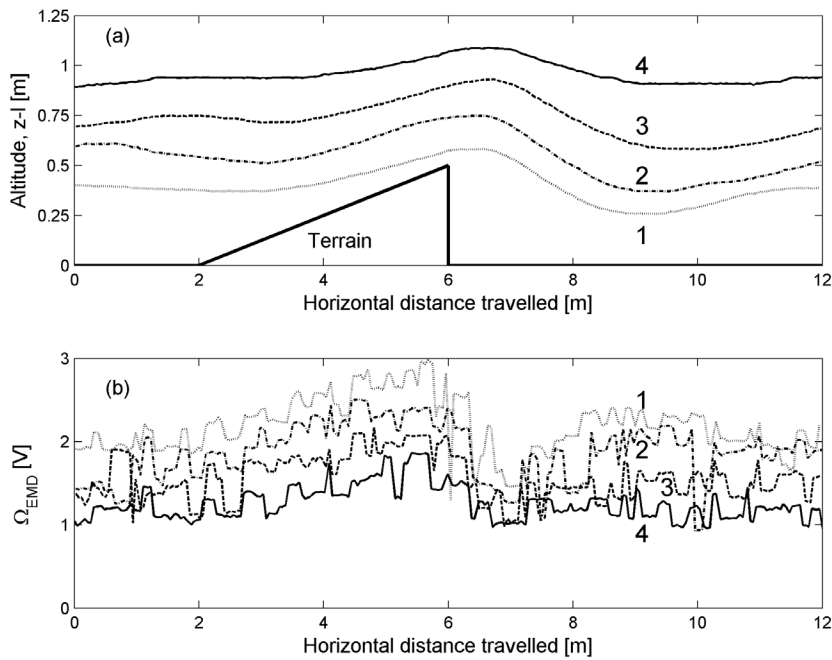


Figure 9. (a) Four trajectories recorded at the same ground speed (1m/s) with different optic flow set points. The robot can be seen to have avoided the terrain smoothly. The lower the optic flow, the higher the altitude at which the rotorcraft follows the terrain (curve 4). (b) EMD output measured during each of the four trajectories shown in (a) ($\Omega_{EMD} = 1V$ corresponds to an $\Omega = 45^\circ/s$, $2V \equiv 80^\circ/s$ and $3V \equiv 160^\circ/s$). The fine structure of these responses reflects the detection by the EMD of the successive sectors on the textured terrain (Figure 6).

5.3. Reliability and reproducibility

The flight trajectories obtained were highly reproducible in spite of the presence of aerodynamic disturbances such as ground effects and air turbulence. This is illustrated by a recording of ten consecutive trajectories (Figure 10) during which the MAV travelled a total distance of 120m in 100 seconds. The OCTAVE system gives reliable results in spite

of the complexity of the overall system (visuo-motor system + aeromechanical system + test-rig). The whirling arm brings about additional inertia but negligible friction.

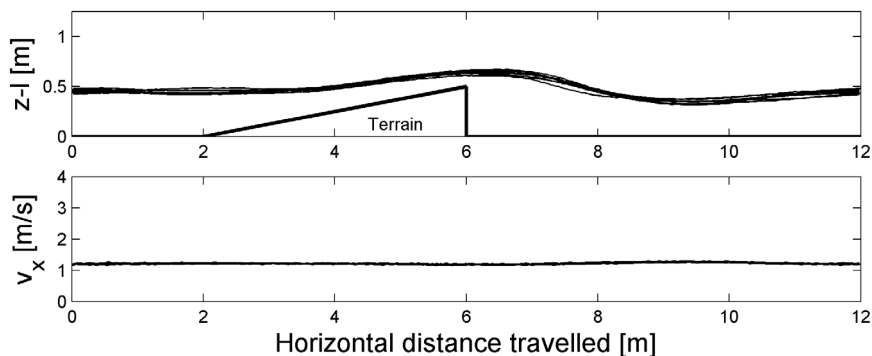


Figure 10. Recording of 10 consecutive trajectories, during which the robot covered a distance of 120 m in 100 seconds at a speed of 1.2m/s without ever crashing. The OCTAVE autopilot gives reproducible, reliable results in the context of a terrain following task.

6. CONCLUSION

Here we presented a quantitative study showing how a tethered 100-gram micro-robotcraft equipped with an elementary optic flow processing system can control its altitude visually by servoing its optic flow. First we showed how the trajectory can be changed by tuning the MAV pitch angle, which determines the ground speed: the higher the ground speed, the higher the altitude will be. A “safe altitude” is thus generated automatically, which increases most appropriately with the ground speed. Secondly, we showed that fine tuning of the optic flow set point determines the robot’s behavior. The higher the optic flow is set, the closer the robot keeps to the ground. At a low optic flow set point, the opposite will occur: the aerial robot will keep far from the ground. Reliable terrain-following is performed in spite of the small occasional errors in the EMD output. The OCTAVE AFCS turned out to be robust and efficient within a given range of forward speeds (1 to 3 m/s). These ground speeds were attained here in open loop via the setting of the MAV pitch angle. The AFCS system is the same at all speeds and does not need to be trimmed to a particular speed. OCTAVE suitably eliminates the “disturbances” caused by an uneven relief and features such as slanting ground.

Unlike most of the autopilots classically used in manned helicopters, the OCTAVE autopilot was not designed to provide the vehicle with altitude holding or ground speed holding capacities. It rather ensures that “optic flow holding” occurs so that the MAV will reach a safe altitude at any speed. The primary advantage of OCTAVE is to make sure that terrain following occurs at all costs without crashing: the result is measured in terms of behavior, and not in terms of variables (speed, height, etc.) measured on-board. The robot behaves appropriately although it would be quite incapable of reporting its groundspeed or its altitude at any time.

The use of a tether was essential for quantitatively implementing and testing the basic strategy used here: optic flow servoing on an elementary rotorcraft with limited (three) degrees of freedom. Tests on free-flying MAVs are more difficult to achieve and lack reproducibility: their results have tended to be more qualitative so far [13]. On the one hand, the whirling arm introduces undesirable inertia into the control loop, which adversely affects both the heave and the surge dynamics: the robot is less agile than it would be if it were flying freely. On the other hand a supporting tether facilitates the parameter monitoring and the understanding of perception/reaction, while making the experiments more reproducible – these are essential points when dealing with proof-of-concept endeavours.

The scheme we have described here for the visual guidance of an aerial vehicle was inspired by the insect world, and the visual processing system itself was inspired by the results of electrophysiological experiments carried out on insects as well. Most present-day computer-vision systems are not up to the task of guiding a micro-air vehicle while meeting the draconian constraints of a total avionic payload of less than 10 grams. Biologically inspired robotics can provide MAVs with well tried and tested alternative solutions, which in some cases may also be scalable to larger UAVs.

The OCTAVE strategy requires remarkably few resources. Once it has been further developed, it promises to give MAVs and UAVs greater autonomy, or to assist a human pilot in their remote operation. After being equipped with an eye with a larger field of view, an OCTAVE-based autopilot could be implemented on-board free-flying 100-gram MAVs, where the eye's pitch counter-rotation could be controlled by a micro vertical gyro. Since obstacle avoidance is also an issue in underwater navigation [34] and planetary exploration, the OCTAVE scheme could also potentially be adapted to benthic submarines and spacecraft, which have to keep some distance from the ground when moving about in uncharted environments.

ACKNOWLEDGEMENTS

We thank Stéphane Viollet for his fruitful comments and suggestions during this work, Marc Boyron for his expert technical assistance and Jessica Blanc for improving the English manuscript. This research was supported by CNRS (Life Science, Engineering Science, Communication and Information Science and Technology, Cogniscience, Microsystem and Microrobotic Programmes) and by an EU contract (IST/FET - 1999- 29043).

REFERENCES

1. J-M. Pichon, C. Blanes and N. Franceschini, "Visual guidance of a mobile robot equipped with a network of self-motion sensors", *SPIE Conf. on Mobile Robots IV*, W.J. Wolfe and W.H. Chun (Eds.), Vol. 1195, pp. 44-53, Bellingham, U.S.A, 1989.
2. N. Franceschini, J-M. Pichon and C. Blanes, "From insect vision to robot vision", *Phil. Trans. Royal. Soc. B*, **337**:283-294, 1992.
3. F. Mura and N. Franceschini, "Visual control of altitude and speed in a flying agent", *From Animals to Animats III*, D. Cliff et al. (Eds.), pp. 91-99, MIT Press, Cambridge, U.S.A, 1994.
4. N. Franceschini, "Engineering Applications of Small Brains", *Future Electron Devices Journal*, **7**(suppl.2):32-47, 1996.
5. S. Viollet and N. Franceschini, "Visual servo system based on a biologically-inspired scanning sensor", *SPIE Conf. on Sensor fusion and decentralized control in Robotics II*, Vol. 3839, pp. 144-155, Bellingham, U.S.A., 1999.
6. T. Netter and N. Franceschini, "Neuromorphic Optical Flow Sensing for Nap-of-the-Earth flight", *SPIE Conf. on Mobile Robots XIV*, Vol. 3838, pp. 208-216, Bellingham, U.S.A., 1999.
7. T. Netter and N. Franceschini, "A Robotic Aircraft that Follows Terrain Using a Neuromorphic Eye", *Proc. of IEEE Conference on Intelligent Robots and Systems (IROS)*, pp. 129-134, Lausanne, Switzerland, 2002.
8. F. Ruffier, S. Viollet, S. Amic and N. Franceschini, "Bio-inspired optical flow circuits for the visual guidance of Micro-Air Vehicles", *Proc. of IEEE International Symposium on Circuits and Systems (ISCAS)*, Vol. III, pp.846-849, Bangkok, Thailand, 2003.
9. F. Ruffier, S. Viollet and N. Franceschini, "OSCAR and OCTAVE : two bio-inspired visually guided aerial micro-robots", *Proc of IEEE 11th International Conference on Advanced Robotics (ICAR)*, pp. 726-732, Coimbra, Portugal, 2003.
10. N. Franceschini, "From Fly Vision to Robot Vision : Re-construction as a mode of discovery", *Sensors and Sensing in Biology and Engineering*, Barth, F.G., Humphrey, J. A., Secomb T.W. (Eds.), pp. 223-235, Springer, Berlin, 2003.
11. Webb, B, "Can robots make good models of biological behaviour?" *Behavioral and Brain Sciences* **24**(6), 2001.
12. T.R. Neumann and H. Bülthoff, "Insect inspired visual control of translatory flight", *Proc. of ECAL 2001*, pp 627-636, Springer, Berlin, 2001.
13. G.L. Barrows, "Future visual microsensors for mini/micro-UAV applications", *Proc. of 7th IEEE International Workshop on Cellular Neural Networks and their Applications*, 2002.
14. M.V. Srinivasan, S.W. Zhang, J. Chahl, E. Barth and S. Venkatesh, "How Honeybees make grazing landings on flat surfaces", *Biological Cybernetics*, **83**(3):171-183, 2000.
15. F. Iida, "Goal-directed navigation of an autonomous flying robot using biologically inspired cheap vision", *Proc. of 32nd Int. Symp. on Robotics*, pp. 1404-1409, Seoul, Korea, 2001.
16. M. Ichikawa, H. Yamada and J. Takeuchi, "Flying robot with biologically inspired vision", *Journal of Robotics and Mechatronics*, **13**:621-624, 2001.
17. S. Saripalli, D. J. Naffin and G. S. Sukhatme, "Autonomous Flying Vehicle Research at the University of Southern California", *In Proceedings of First International Workshop on Multi-Robot Systems*, Washington DC, USA, 2002.

18. C.S. Sharp, O. Shakernia and S.S. Sastry, "A Vision System For Landing an Unmanned Aerial Vehicle", *In Proceedings of IEEE International Conference on Robotics and Automation (ICRA)*, pp. 1720-1727, Seoul, Korea, 2001.
19. O. Amidi, T. Kanade, and J.R. Miller, "Vision-Based Autonomous Helicopter Research at Carnegie Mellon Robotics Institute 1991-1997", *American Helicopter Society International Conference*, Gifu, Japan, 1998.
20. J.R. Miller, O. Amidi, C. Thorpe, and T. Kanade, "Precision 3-D modeling for autonomous helicopter flight", *Int. Symp. Robotics Research (ISRR)*, Snowbird, USA, 1999.
21. T. Collett, H. Nalbach and H. Wagner, "Visual stabilization in arthropods", *Visual Motion and its Role in the stabilization of Gaze*, F.A. Miles, J. Wallman (eds.), pp. 239-263, Elsevier, 1993.
22. W. Reichardt and R. Poggio, "Visual control of orientation behavior in the fly", *Quarterly Reviews of Biophysics*, **9(3)**:311-375, 1976.
23. K. Hausen, "The lobula-complex of the fly : structure, function and significance in visual behaviour", *Photoreception and Vision in Invertebrates*, M. A. Ali (eds.), pp 523-559, Plenum, New York, 1984.
24. N. Franceschini, C. Blanes and L. Oufar, "Passive, non-contact optical velocity sensor" (in French), *Dossier technique ANVAR/DVAR N°51 549*, Paris, 1986.
25. C. Blanes, "Appareil visuel élémentaire pour la navigation à vue d'un robot mobile autonome", DEA thesis (Neurosciences), Univ. Aix-Marseille, 1986.
26. N. Franceschini, A. Riehle and A. Le Nestour, "Directionally Selective Motion Detection by Insect Neurons", *Facets of vision*, D.G. Stavenga, R.C. Hardie (eds.), pp. 360-390, Springer, Berlin, 1989.
27. J.J. Gibson, *The Ecological Approach to Visual Perception*, Boston: Houghton Mifflin, 1979.
28. J. S. Kennedy, "The migration of the desert locust (*Schistocerca gregaria* Forsk.)", *Phil. Trans. Royal Soc. B*, **235**:163-290, 1951.
29. C. T. David, "The relationship between body angle and flight speed in free-flying *Drosophila*", *Physiol. Ent.*, **3**:191-195, 1978.
30. K.G. Götz, "Die optischen Übertragungseigenschaften der Komplexaugen von *Drosophila*", *Kybernetik*, **2**:215-221, 1965.
31. S. Ullman, "Analysis of Visual Motion by Biological and Computer Systems", *IEEE Computer*, pp. 58-69, 1981.
32. W. Reichardt, "Movement perception in insects", *Processing of Optical data by organisms and by machines*, W. Reichardt (ed), pp 465-493, New York: Academic Press, 1969.
33. J.-M Pichon, *Guidage visuel d'un robot mobile autonome d'inspiration biologique*, PhD Thesis, National Polytechnic Institute, Grenoble, 1991.
34. V. Creuze and Jouvencel B., "Avoidance of Underwater Cliffs for Autonomous Underwater Vehicles", *Proc. of IEEE Conference on Intelligent Robots and Systems (IROS)*, pp. 793-798, Lausanne, Switzerland, 2002.